Journal of Materials Chemistry B

RSC Publishing

PAPER

View Article Online
View Journal | View Issue

Cite this: J. Mater. Chem. B, 2013, 1, 5762

Dye-enhanced graphene oxide for photothermal therapy and photoacoustic imaging†

Yi-Wei Wang,[a] Yu-Ying Fu,[a] Qiaoli Peng,[b] Shan-Shan Guo,[a] Gang Liu,[b] Juan Li,*[a] Huang-Hao Yang*[a] and Guo-Nan Chen[a]

Received 17th July 2013
Accepted 9th September 2013

DOI: 10.1039/c3tb20986e

www.rsc.org/MaterialsB

Graphene oxide (GO) has many exciting advantages such as easy preparation, low toxicity, good solubility and stability in aqueous solution. However, GO itself has a low near-infrared (NIR) absorption, and thus is not suitable for photothermal therapy and photoacoustic imaging. To overcome this limitation, a novel dye-enhanced GO is prepared utilizing the π–π stacking interactions between GO and indocyanine green (ICG). The ICG–GO complex has a high optical absorbance in the NIR region and exhibits excellent photothermal properties under NIR irradiation. In order to improve the cancer-targeting activity, GO was modified with folic acid (FA). *In vitro* experiments showed that the ICG–GO–FA nanocomposite could be used for targeted photothermal cancer cell destruction. Moreover, the application of the ICG–GO–FA nanocomposite for photoacoustic imaging was also demonstrated.

1. Introduction

Cancer is a major public health problem in the United States and many other parts of the world. A total of 1 660 290 new cancer cases and 580 350 cancer deaths are projected to occur in the United States in 2013.[1] It is therefore necessary to develop efficient methods for the treatment of cancer. Photothermal therapy (PTT) is a promising treatment modality for cancers and other malignant diseases in a minimally invasive manner. In this treatment, NIR-absorbing photothermal agents are first delivered to targeted cells or tissues and then irradiated with a NIR laser which can penetrate relatively deep into tissues without damaging normal biological tissues. The absorbed light is then converted to heat and transferred to the cell environment, generating localized hyperthermia and destroying cancer cells. Recently, there has been an explosion of interest in the development of nanomaterials for photothermal therapy due to their improved NIR-absorption, photo-stability or photothermal conversion efficiency. Examples of these materials include organic nanoparticles,[2–5] gold nanostructures,[6–9] copper chalcogenide semiconductors,[10,11] Pd nanosheets[12] as well as carbon nanotubes.[13,14]

Graphene, a single layer of carbon atoms, has attracted great attention recently.[15] Until now, several methods have been successfully established for the synthesis of graphene and its derivatives. In the biomedical area,[16–18] such as biosensing[19–22] and drug delivery,[23,24] the most commonly used derivatives of graphene are graphene oxide (GO) and reduced graphene oxide (RGO), due to their biocompatibility and easy synthesis at a large scale and low cost. GO can be easily prepared from native graphite flakes according to the modified Hummers' method.[25] After chemical reduction, GO can be transformed into RGO. RGO has high NIR absorption and is reported to be a potential photothermal agent for treatment of diseases, such as cancer,[26–29] Alzheimer's disease[30] and bacterial infection.[31,32] Compared with RGO, GO offers several advantages. First, GO is practically non-toxic at certain concentration levels.[33,34] In contrast, the surface of RGO is highly hydrophobic, and thus it is considered more toxic than the unreduced GO.[35–37] Second, GO contains hydrophilic functional groups that enable chemical functionalization and water-solubility. Third, GO is easier to degrade than RGO.[38] The recent findings on the possible biodegradability of GO are another positive factor for GO to be used *in vivo*.[39] However, the NIR absorption of GO is much lower than that of RGO, and thus GO itself is not suitable for photothermal therapy.

Imaging techniques, based on targeted contrast agents are also very important for earlier detection of tumors, understanding the distribution of photoabsorbers in tumors and other organs, as well as assessing the therapeutic efficacy and monitoring the post-treatment tumor behaviors.[40] Photoacoustic tomography (PAT) is a novel hybrid imaging modality that is based on the detection of acoustic waves generated by absorption of pulsed light by tissue chromophores or targeted

[a]The Key Lab of Analysis and Detection Technology for Food Safety of the MOE, Fujian Provincial Key Laboratory of Analysis and Detection Technology for Food Safety, College of Chemistry and Chemical Engineering, Fuzhou University, Fuzhou 350108, P.R. China

[b]Center for Molecular Imaging and Translational Medicine, School of Public Health, Xiamen University, Xiamen, Fujian, 361002, China. E-mail: hhyang@fio.org.cn; Fax: +86 591 22866227; Tel: +86 591 22866135

† Electronic supplementary information (ESI) available. See DOI: 10.1039/c3tb20986e

contrast agents. PAT has high contrast and good spatial resolution. In addition, due to the intrinsic character of the employed NIR light and generated ultrasonic signal, PAT is believed to offer more accuracy than other imaging modalities for guiding PTT.

Indocyanine green (ICG) is a Federal Drug Administration approved agent for clinical NIR fluorescence imaging.[41] Because of its intrinsic strong NIR absorption, ICG has also been used to selectively increase the photothermal destructions in the target tumors.[42] However, most of the light-absorbing dyes including ICG have some limitations, such as concentration-dependent aggregation, poor photo-stability, non-specific binding to proteins, lack of target specificity and short half-life in the circulation.[43] There are some reports on the improvement of the stability of ICG.[44,45] Encouraged by the good solubility of GO and strong NIR absorption ability of ICG, we predicted that by the combination of GO with ICG, a new ICG–GO complex can be formed and used as a promising material for clinical diagnosis and therapy of cancer.

Herein, we proved that the ICG–GO complex can be used as a novel NIR-absorbing agent for photothermal therapy and a good contrast agent for photoacoustic imaging. ICG–GO was prepared by simply mixing GO with ICG. It was found that the obtained ICG–GO possessed good photostability and an excellent photothermal property. In order to improve the cancer-targeting activity, ICG–GO was modified with folic acid (FA) which targeted a variety of tumor cells over-expressing the folate receptor (FR). *In vitro* experiments showed that ICG–GO–FA was very biocompatible and exhibited non-cytotoxicity without NIR irradiation. In contrast, in the presence of NIR irradiation, ICG–GO–FA can be used for targeted photothermal ablation of cancer cells. Photoacoustic imaging using ICG–GO was also performed. Our results showed that ICG–GO could also be used as a good photoacoustic contrast agent.

2. Materials and methods

2.1. Materials and apparatus

Graphite powder (analytical grade) was purchased from Sinopharm Chemical Reagent Co. Ltd (China). 3-(4,5-Dimethylthiazol-2-yl)-2,5-diphenyltetrazolium bromide (MTT), 1-ethyl-3-(3-dimethylaminopropyl) carbodiimide hydrochloride (EDC), *N*-hydroxysulfosuccinimide (NHS), ICG and FA were purchased from Sigma-Aldrich. All the other chemicals were of analytical grade and were used as received.

UV-vis absorption spectra were recorded using a SH-1000 Lab microplate reader (Corona Electric, Hitachinaka, Japan) at room temperature. Atomic force microscopy (AFM) measurement was performed with a Multimode 3D atomic force microscope (Bruker Nano Inc., USA). A semiconductor laser unit (KS3-11312-110, BWT, Beijing Kaipulin Co. Ltd, China) was used for photothermal irradiation.

2.2. Preparation of ICG–GO

GO was synthesized from graphite powder by a modified Hummers method.[25] Then, the solution of GO was centrifuged at 10 000 rpm for 10 min to remove any large size GO sheets. The supernatant was collected. ICG (5 mg mL^{-1}) was dissolved in DMSO first and then added to GO water solutions (the final concentration of both GO and ICG is 0.5 mg mL^{-1}). Then the solution was agitated overnight in the dark at 4 °C. Unbound ICG molecules were removed from the solution by filtration through 10 kDa centrifuge filters (Millipore) and washed for 6–8 times.

2.3. Preparation of RGO

To prepare RGO, hydrazine hydrate (~100 μL) was added to the GO solution (10 mL) at a concentration of ~1 mg mL^{-1} and heated in an oil bath at 95 °C under stirring for 30 min. The GO solution changed color from yellow to black during the reduction step, indicating increased light absorption in the visible and NIR region. The obtained RGO was characterized by Raman spectroscopy on a Renishaw inVia Raman microspectrometer at room temperature.

2.4. Synthesis of NH_2–PEG_{2000}–FA

FA was conjugated with NH_2–PEG_{2000}–NH_2 *via* EDC/NHS chemistry. Typically, FA (0.01 mmol), EDC (0.05 mmol), and NHS (0.03 mmol) were dissolved in DMSO (5 mL) under vigorous stirring and maintained at room temperature for 1 h. Then, the mixture solution was added to a dry solution of NH_2–PEG_{2000}–NH_2 (20 mg) in 5 mL DMSO through a dropping funnel at a rate of 0.5 drop per s and maintained at room temperature for 12 h. DMSO was removed by distillation at 60 °C under reduced pressure. The residual was dissolved in anhydrous THF. Next, the resulting product was isolated by filtration to remove the free FA, and then precipitated in anhydrous ethyl ether to obtain the final product NH_2–PEG_{2000}–FA.

2.5. Preparation of ICG–GO–FA

GO (10 mL, 0.5 mg mL^{-1}) was first mixed with NH_2–PEG_{2000}–FA (5 mg) in an ultrasound bath for 10 min; after the addition of 5 mg EDC and 3 mg NHS, the reaction mixture was kept stirring for 24 h at room temperature. The surface decorated GO–FA was obtained by dialysis in a 10 kDa dialysis bag against deionized water. Next, GO–FA (GO concentration 0.5 mg mL^{-1}) was incubated with ICG molecules (0.5 mg mL^{-1}) overnight to form ICG–GO–FA. Unbound ICG molecules were removed by ultrafiltration.

2.6. Photothermal effect measurement

To study the photothermal effect induced by the NIR irradiation, 1 mL aqueous solutions containing different materials were irradiated by a NIR laser (808 nm, 1 W) for 10 min. The temperatures of the solutions were monitored by a thermocouple microprobe ($\varphi = 0.5$ mm) submerged in the solution in a 1 cm square cuvette. The probe was placed at such a position that the direct irradiation of the laser on the probe was avoided. The tip of the thermocouple was ~5 mm above the bottom of the cuvette.

2.7. *In vitro* photothermal therapy

To investigate the cancer cell killing efficiency of ICG–GO and ICG–GO–FA under laser irradiation, Hela cells were incubated with these composites at the same GO concentration (20 μg mL^{-1}) under 37 °C for 1 h. After washing with phosphate buffer for 3 times to remove the unbound composites, cells were exposed to an NIR laser (808 nm) at a power density of 2 W cm^{-2}. At last, a standard cell viability assay using MTT was conducted.

2.8. Photoacoustic imaging

To test the linearity of the photoacoustic signal as a function of ICG–GO concentration, we used an agar-phantom with no scattering or absorbing additives. ICG–GO at increasing weight was mixed with warm liquid agar in multiples of 3 forming ICG–GO solutions at 0.125, 0.25, 0.5, 1, 2 μg. Inclusions 2–3 mm deep were made in the agar phantom and ~100 μL of ICG–GO solution was poured into the well. Upon solidification of the gel, another layer of ~3 mm liquid agarose was poured on top of the phantom. A complete photoacoustic image of the phantom was acquired at 808 nm. 3D cylindrical ROIs at the size of the inclusion were used to estimate the photoacoustic signal from each well.

To compare the performance of plain ICG–GO and GO–FA to ICG–GO–FA, we incubated increasing numbers of Hela cells with ICG–GO, GO–FA and ICG–GO–FA respectively for a 1 h period. After incubation, the cells were washed with cold saline to remove unbound composites and then span down for 3 min at 1500 rpm to remove excess liquid. We repeated this washing process twice. The cells were then placed in an agarose phantom at increasing numbers from 3×10^4 to 5×10^5 cells per well. The agarose phantom was created in a similar way to the other agarose phantoms mentioned above in this work (1% ultrapure agarose, 99% DI water by weight). The wells in the agarose phantom were made using a pipette tip. We mixed the cell solution with warm agarose liquid and poured into the wells of the agarose phantom. After 5–10 minutes the cell–agarose solution solidified into the well and an additional liquid agarose layer was deposited on the entire phantom to "seal" the wells and protect the content of the wells. The phantom was then positioned inside a water tank and a full 3D scan of the phantom was taken using a photoacoustic instrument (Endra, Nexus 128) at 808 nm wavelength. Quantitative analysis of the photoacoustic signal from the phantom was done using the OSIRIX software by drawing 3D regions of interest around each inclusion.

3. Results and discussions

3.1. Preparation and characterization of ICG–GO and ICG–GO–FA

Fig. 1a shows the illustration of ICG–GO–FA preparation and application. GO was synthesized from graphite powder as depicted in Section 2.2. Fig. 1b shows an AFM image of the synthesized GO. The sizes of the GO sheets were ~200 nm. Tapping mode atomic force microscopy was used to determine the thickness of the GO. The thickness of the GO sheets was

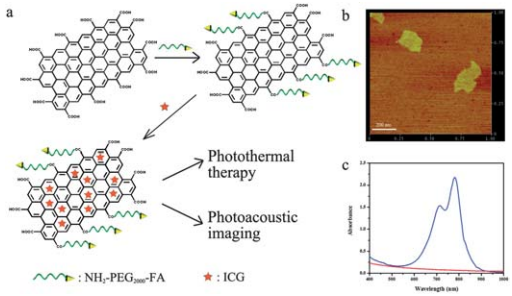

Fig. 1 ICG–GO–FA preparation and characterization. (a) A schematic illustration of ICG–GO–FA preparation and application. (b) An AFM image of GO (scale bar represents 200 nm). (c) Absorption spectra of ICG–GO (blue) and GO (red).

~1 nm, indicating that the synthesized GO was single-layered. ICG molecules have four aromatic groups and four double bonds in the carbon chain between two polycyclic parts which are capable of forming strong π–π stacking interactions with GO. Therefore, ICG–GO can be simply prepared through mixing GO solution with ICG. The optical absorptions of GO and ICG–GO were recorded. Fig. 1c indicates that ICG–GO showed ~20 times higher optical absorption than GO alone at 808 nm. ICG–GO was also characterized with fluorescence spectroscopy. In the characterization, the amount of GO was changed while the concentration of ICG was fixed. As shown in Fig. S1,† the fluorescence of ICG decreased as the concentration of GO increased. Almost 100% quenching of fluorescence was observed when the weight of GO equaled that of ICG. This observation indicates strong adsorption of ICG on GO. In order to further investigate the stability of ICG–GO, the ICG–GO complex was dispersed in cell culture media containing fetal bovine serum in the dark for 3 hours. After that, the fluorescence of ICG was measured to check the release of ICG from the ICG–GO complex. Little fluorescence recovery (less than 5%) was observed (Fig. S2†), indicating that the ICG–GO complex is very stable.

3.2. Comparison of the photothermal effect of different materials

To verify the potential usage of ICG–GO in PTT, the photothermal effect of different materials (GO, ICG, ICG–GO, and RGO) has been compared. The results are shown in Fig. 2. An ICG–GO solution (GO concentration 20 μg mL^{-1}) was exposed to an 808 nm NIR laser at a power density of 1 W cm^{-2} with GO aqueous solution (20 μg mL^{-1}) as the control. From Fig. 2, a small temperature increase of the GO solution could be observed (curve D), indicating the poor photothermal property of GO. We also tested the photothermal effect of ICG (curve C). It can be observed that the photostability of ICG is poor. After 5 min of irradiation, the color of ICG solution changed from green to yellow and the solution temperature began to decrease, which indicated the degradation of ICG. A rapid temperature increase of the ICG–GO solution was observed when exposed to the laser (curve A). At the same time, the adsorption of ICG onto GO can prevent the decomposition of ICG. For comparison, the temperature of hydrazine hydrate-reduced graphene oxide

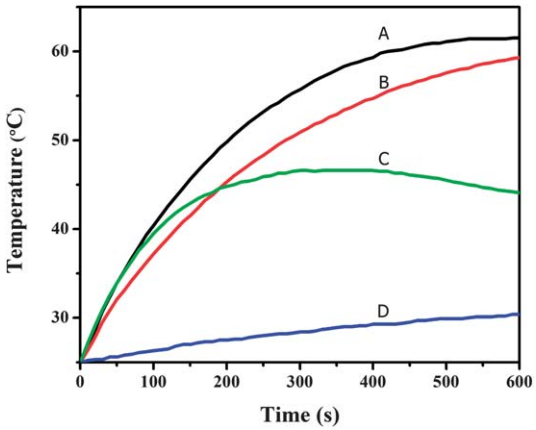

Fig. 2 Temperature change curves of (A) ICG–GO, (B) RGO, (C) ICG and (D) GO solutions exposed to the 808 nm laser at a power density of 1 W cm^{-2}.

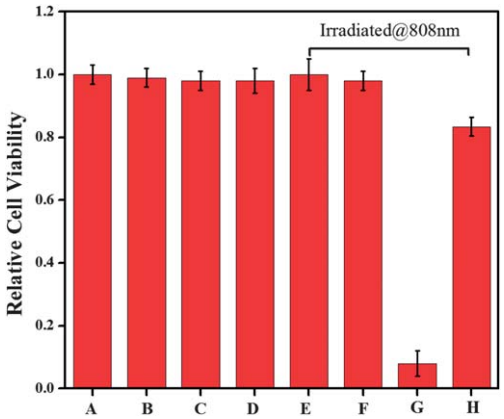

Fig. 3 Cytotoxicity of (A) control, (B) GO–FA, (C) ICG–GO–FA, (D) ICG–GO to cancer cells and photothermal ablation of cancer cells based on (E) control, (F) GO–FA, (G) ICG–GO–FA, (H) ICG–GO.

(RGO, 20 μg mL^{-1}) solution treated with the same irradiation condition was also recorded (curve B). It can be seen that the photothermal effect of ICG–GO is comparable to that of RGO prepared by our group and that reported in the literature[29] (Fig. S3†) and is better than that of ICG–SWNT.[46] After laser irradiation, the fluorescence of ICG–GO solution was measured immediately. No obvious fluorescence recovery was observed (Fig. S2†). This suggests that laser irradiation does not result in the release of ICG from the ICG–GO complex. These results demonstrated that ICG–GO exhibited an excellent photothermal property and good photostability.

3.3. Cellular photothermal therapy

Motivated by the strong NIR absorbance and highly effective photothermal heating of ICG–GO, we then carried out an *in vitro* photothermal therapy study. In order to improve the cancer-targeting, GO was modified with FA. Hela cells were incubated in a solution of GO–FA, ICG–GO or ICG–GO–FA at the same GO concentration (20 μg mL^{-1}) for 1 h. Before or after 808 nm NIR laser (2 W cm^{-2}, 10 min) irradiation, photothermal ablation of Hela cells was confirmed by MTT experiments; the results are shown in Fig. 3. Before irradiation, the incubation of Hela cells with GO–FA, ICG–GO or ICG–GO–FA only resulted in a smaller decrease of cell viabilities (Fig. 3B, C and D) than the control (Fig. 3A), indicating that GO–FA, ICG–GO and ICG–GO–FA are less toxic and highly biocompatible. As expected, the NIR irradiation alone did not inhibit cell viability (Fig. 3E), suggesting that the irradiation of NIR light is relatively harmless. In contrast, the viabilities of Hela cells that were irradiated with NIR light after incubation with ICG–GO–FA decreased to 8% (Fig. 3G). FA, a well-known low molecular weight vitamin, is targeted to FR that is overexpressed on a wide range of human cancers such as Hela cells. It is found that without FA or ICG, the therapy effect is greatly limited (Fig. 3F). These results demonstrated successful targeting and photothermal killing of the Hela cells using ICG–GO–FA. Therefore, we believe that ICG–GO–FA is a promising agent for targeted photothermal ablation of cancer cells *in vivo*.

3.4. Cellular photoacoustic imaging

As is reported by many groups, materials with a photothermal effect usually can be used as contrast agents for photoacoustic imaging.[47,48] We found that ICG–GO can also be used as a contrast agent for photoacoustic imaging. We constructed a non-absorbing and non-scattering agarose phantom with inclusions of ICG–GO at increasing weight from 125 ng to 2 μg in multiples of 3. As shown in Fig. 4, the photoacoustic signal of ICG–GO increased with increase of GO weight. The photoacoustic signal produced by ICG–GO correlated highly with GO weight ($R = 0.99$), suggesting that ICG–GO is an excellent candidate for contrast enhancement for PAT. Furthermore, cell uptake studies revealed that ICG–GO–FA showed a good contrast enhancement to Hela cells while ICG–GO and GO–FA failed to show satisfactory contrast enhancement (Fig. 5). This maybe due to the fact that ICG–GO is not able to target Hela cells and GO–FA has a much lower NIR absorption than ICG–GO–FA.

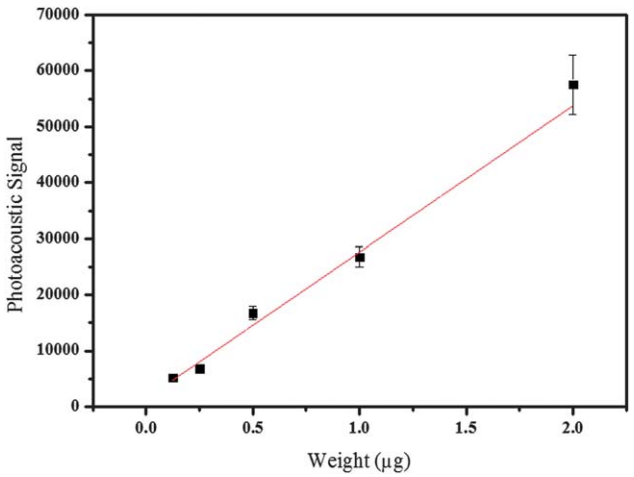

Fig. 4 The photoacoustic signal produced by ICG–GO was observed to be linearly dependent on the GO concentration.

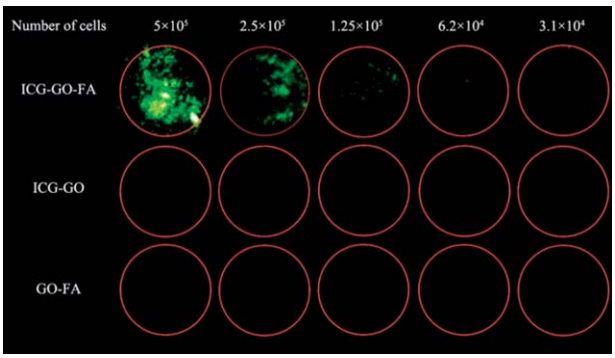

Fig. 5 Photoacoustic images of Hela cells using ICG–GO–FA, ICG–GO or GO–FA as a contrast agent.

4. Conclusions

In summary, a novel ICG–GO–FA nanocomposite was prepared and used for effective PTT therapy and PAT imaging of cancer cells based on its excellent photothermal effect and photoacoustic effect. Through adsorption of ICG, ICG–GO showed ~20 times higher optical absorption compared with GO alone at 808 nm. The prepared ICG–GO exhibits excellent photothermal properties and photostability under NIR irradiation. Successful targeting and photothermal killing of the targeted cells using ICG–GO–FA was demonstrated. Moreover, the applications of dye-enhanced GO as ultrahigh sensitive photoacoustic imaging agents were also demonstrated. Given its cost-effectiveness, easy fabrication and low cytotoxicity, ICG–GO–FA would be a promising candidate for photothermal therapy and photoacoustic imaging of cancers *in vivo*.

Acknowledgements

The authors gratefully acknowledge the financial support from the National Basic Research Program of China (no. 2010CB732403), the National Natural Science Foundation of China (no. 21125524, no. 20975023), the Program for New Century Excellent Talents in the University of China (no. 09-0014), the Program for Changjiang Scholars and Innovative Research Team in University (no. IRT1116) and the National Science Foundation of Fujian Province (no. 2010J06003).

Notes and references

1 R. Siegel, D. Naishadham and A. Jemal, *Ca-Cancer J. Clin.*, 2013, **63**, 11–30.
2 L. Cheng, K. Yang, Q. Chen and Z. Liu, *ACS Nano*, 2012, **6**, 5605–5613.
3 K. Yang, H. Xu, L. Cheng, C. Sun, J. Wang and Z. Liu, *Adv. Mater.*, 2012, **24**, 5586–5592.
4 Y. Liu, K. Ai, J. Liu, M. Deng, Y. He and L. Lu, *Adv. Mater.*, 2013, **25**, 1353–1359.
5 Z. Zha, X. Yue, Q. Ren and Z. Dai, *Adv. Mater.*, 2013, **25**, 777–782.
6 C. Loo, A. Lowery, N. J. Halas, J. West and R. Drezek, *Nano Lett.*, 2005, **5**, 709–711.
7 Y.-F. Huang, K. Sefah, S. Bamrungsap, H.-T. Chang and W. Tan, *Langmuir*, 2008, **24**, 11860–11865.
8 X. H. Huang, I. H. El-Sayed, W. Qian and M. A. El-Sayed, *J. Am. Chem. Soc.*, 2006, **128**, 2115–2120.
9 Y. Ma, X. Liang, S. Tong, G. Bao, Q. Ren and Z. Dai, *Adv. Funct. Mater.*, 2013, **23**, 815–822.
10 Y. Li, W. Lu, Q. Huang, M. Huang, C. Li and W. Chen, *Nanomedicine*, 2010, **5**, 1161–1171.
11 C. M. Hessel, V. P. Pattani, M. Rasch, M. G. Panthani, B. Koo, J. W. Tunnell and B. A. Korgel, *Nano Lett.*, 2011, **11**, 2560–2566.
12 S. Tang, X. Huang and N. Zheng, *Chem. Commun.*, 2011, **47**, 3948–3950.
13 J. T. Robinson, K. Welsher, S. M. Tabakman, S. P. Sherlock, H. Wang, R. Luong and H. Dai, *Nano Res.*, 2010, **3**, 779–793.
14 L. Wang, J. Shi, H. Zhang, H. Li, Y. Gao, Z. Wang, H. Wang, L. Li, C. Zhang, C. Chen, Z. Zhang and Y. Zhang, *Biomaterials*, 2013, **34**, 262–274.
15 K. S. Novoselov, A. K. Geim, S. V. Morozov, D. Jiang, Y. Zhang, S. V. Dubonos, I. V. Grigorieva and A. A. Firsov, *Science*, 2004, **306**, 666–669.
16 K. S. Novoselov, V. I. Fal'ko, L. Colombo, P. R. Gellert, M. G. Schwab and K. Kim, *Nature*, 2012, **490**, 192–200.
17 Y. Wang, Z. Li, J. Wang, J. Li and Y. Lin, *Trends Biotechnol.*, 2011, **29**, 205–212.
18 H. Zhang, G. Gruener and Y. Zhao, *J. Mater. Chem. B*, 2013, **1**, 2542–2567.
19 C.-H. Lu, H.-H. Yang, C.-L. Zhu, X. Chen and G.-N. Chen, *Angew. Chem., Int. Ed.*, 2009, **48**, 4785–4787.
20 S. Guo and S. Dong, *Chem. Soc. Rev.*, 2011, **40**, 2644–2672.
21 Y. Tao, Y. Lin, Z. Huang, J. Ren and X. Qu, *Adv. Mater.*, 2013, **25**, 2594–2599.
22 X. Chen, Z. Cai, Z. Huang, M. Oyama, Y. Jiang and X. Chen, *Nanoscale*, 2013, **5**, 5779–5783.
23 Z. Liu, J. T. Robinson, X. Sun and H. Dai, *J. Am. Chem. Soc.*, 2008, **130**, 10876.
24 C. H. Lu, C. L. Zhu, J. Li, J. J. Liu, X. Chen and H. H. Yang, *Chem. Commun.*, 2010, **46**, 3116–3118.
25 W. S. Hummers and R. E. Offeman, *J. Am. Chem. Soc.*, 1958, **80**, 1339.
26 K. Yang, S. Zhang, G. Zhang, X. Sun, S. T. Lee and Z. Liu, *Nano Lett.*, 2010, **10**, 3318–3323.
27 O. Akhavan, E. Ghaderi, S. Aghayee, Y. Fereydooni and A. Talebi, *J. Mater. Chem.*, 2012, **22**, 13773–13781.
28 J. T. Robinson, S. M. Tabakman, Y. Liang, H. Wang, H. S. Casalongue, D. Vinh and H. Dai, *J. Am. Chem. Soc.*, 2011, **133**, 6825–6831.
29 K. Yang, J. Wan, S. Zhang, B. Tian, Y. Zhang and Z. Liu, *Biomaterials*, 2012, **33**, 2206–2214.
30 M. Li, X. Yang, J. Ren, K. Qu and X. Qu, *Adv. Mater.*, 2012, **24**, 1722–1728.
31 Y.-W. Wang, Y.-Y. Fu, L.-J. Wu, J. Li, H.-H. Yang and G.-N. Chen, *J. Mater. Chem. B*, 2013, **1**, 2496.
32 M.-C. Wu, A. R. Deokar, J.-H. Liao, P.-Y. Shih and Y.-C. Ling, *ACS Nano*, 2013, **7**, 1281–1290.

33 A. Bianco, *Angew. Chem., Int. Ed.*, 2013, **52**, 4986–4997.
34 I. E. Mejias Carpio, C. M. Santos, X. Wei and D. F. Rodrigues, *Nanoscale*, 2012, **4**, 4746–4756.
35 A. Sasidharan, L. S. Panchakarla, P. Chandran, D. Menon, S. Nair, C. N. Rao and M. Koyakutty, *Nanoscale*, 2011, **3**, 2461–2464.
36 O. Akhavan and E. Ghaderi, *ACS Nano*, 2010, **4**, 5731–5736.
37 W. Hu, C. Peng, W. Luo, M. Lv, X. Li, D. Li, Q. Huang and C. Fan, *ACS Nano*, 2010, **4**, 4317–4323.
38 G. P. Kotchey, S. A. Hasan, A. A. Kapralov, S. H. Ha, K. Kim, A. A. Shvedova, V. E. Kagan and A. Star, *Acc. Chem. Res.*, 2012, **45**, 1770–1781.
39 G. P. Kotchey, B. L. Allen, H. Vedala, N. Yanamala, A. A. Kapralov, Y. Y. Tyurina, J. Klein-Seetharaman, V. E. Kagan and A. Star, *ACS Nano*, 2011, **5**, 2098–2108.
40 L. Cheng, K. Yang, Y. Li, X. Zeng, M. Shao, S. T. Lee and Z. Liu, *Biomaterials*, 2012, **33**, 2215–2222.
41 V. L. Dzurinko, A. S. Gurwood and J. R. Price, *Optometry – Journal of the American Optometric Association*, 2004, **75**, 743–755.
42 W. R. Chen, H. Liu, J. W. Ritchey, K. E. Bartels, M. D. Lucroy and R. E. Nordquist, *Cancer Res.*, 2002, **62**, 4295–4299.
43 V. Saxena, M. Sadoqi and J. Shao, *J. Pharm. Sci.*, 2003, **92**, 2090–2097.
44 X. Zheng, D. Xing, F. Zhou, B. Wu and W. R. Chen, *Mol. Pharm.*, 2011, **8**, 447–456.
45 A. de la Zerda, Z. Liu, S. Bodapati, R. Teed, S. Vaithilingam, B. T. Khuri-Yakub, X. Chen, H. Dai and S. S. Gambhir, *Nano Lett.*, 2010, **10**, 2168–2172.
46 X. Zheng and F. Zhou, *J. X-Ray Sci. Technol.*, 2011, **19**, 275–284.
47 Z. Zha, S. Zhang, Z. Deng, Y. Li, C. Li and Z. Dai, *Chem. Commun.*, 2013, **49**, 3455–3457.
48 W. Lu, M. P. Melancon, C. Xiong, Q. Huang, A. Elliott, S. Song, R. Zhang, L. G. Flores, 2nd, J. G. Gelovani, L. V. Wang, G. Ku, R. J. Stafford and C. Li, *Cancer Res.*, 2011, **71**, 6116–6121.